# Kinetics of Hexagonal Cylinders to Face-centered Cubic Spheres Transition of Triblock Copolymer in Selective Solvent: Brownian Dynamics Simulation

**DATASET** · FEBRUARY 2015

READS
21

**3 AUTHORS:**

Minghai li
Northeastern University
**32** PUBLICATIONS **150** CITATIONS
SEE PROFILE

Yongsheng Liu
China University of Petroleum
**188** PUBLICATIONS **3,757** CITATIONS
SEE PROFILE

Rama Bansil
Boston University
**129** PUBLICATIONS **2,405** CITATIONS
SEE PROFILE

# Kinetics of hexagonal cylinders to face-centered cubic spheres transition of triblock copolymer in selective solvent: Brownian dynamics simulation[a)]

Minghai Li,[b)] Yongsheng Liu, and Rama Bansil[c)]
*Department of Physics, Boston University, Boston, Massachusetts 02215, USA*

(Received 13 April 2010; accepted 9 July 2010; published online 26 August 2010)

The kinetics of the transformation from the hexagonal packed cylinder (hex) phase to the face-centered-cubic (fcc) phase was simulated using Brownian dynamics for an ABA triblock copolymer in a selective solvent for the A block. The kinetics was obtained by instantaneously changing either the temperature of the system or the well-depth of the Lennard-Jones potential. Detailed analysis showed that the transformation occurred via a rippling mechanism. The simulation results indicated that the order-order transformation was a nucleation and growth process when the temperature of the system instantly jumped from 0.8 to 0.5. The time evolution of the structure factor obtained by Fourier transformation showed that the peak intensities of the hex and fcc phases could be fit well by an Avrami equation. © *2010 American Institute of Physics*.
[doi:10.1063/1.3473067]

## I. INTRODUCTION

It is well known that block copolymers exhibit a rich phase diagram with different ordered phases, such as three-dimensional body-centered-cubic (bcc)/face-centered-cubic (fcc) and the more complicated Gyroid and other bicontinuous phases, two-dimensional hexagonal packed cylinder (hex), and one-dimensional lamellar (LAM) phases.[1–4] A variety of self-assembled micellar domain shapes (spherical, cylindrical, or planar sheets) can be obtained from a block copolymer by varying the composition of and number of blocks, or by varying the polymer concentration, temperature, and solvent selectivity in a block copolymer of fixed composition. Block copolymers, such as lyotropic liquid crystals, offer a unique system to investigate transformations that simultaneously involve a change in the shape of the micellar domains and the symmetry of the underlying lattice, for example, from hex cylinders to bcc spheres. While there are many studies of the equilibrium phase diagrams and thermodynamics of solvent mediated interactions in block copolymer systems, the kinetics is not so well understood. A few experimental studies have been reported on the kinetics of the hex cylinders to bcc spheres transition.[5–8] The kinetics of phase transition in block copolymer melts has been investigated theoretically using self-consistent field theory,[9–13] time-dependent self-consistent field approach,[14] as well as the time-dependent Ginzburg–Landau calculations.[15] Anisotropic fluctuations have been proposed and investigated for the transition from cylinders to spheres in block copolymer melts.[10,12,16] Previous theoretical studies on the kinetics of cylinders-spheres order-order phase transition (OOT) in diblock copolymers focused on hex-bcc transition. To the best of our knowledge, there is no published report on the kinetics of hex cylinders to fcc spheres.

Computational simulation methods can provide the microscopic structural changes involved in the transformation between different phases. Several simulation studies of block copolymers using molecular dynamics (MD),[17–20] discrete MD,[21] Brownian dynamics (BD),[22,23] Monte Carlo,[24–26] and dissipative particle dynamics (DPD),[27] have been reported. In this paper, we report a computational study on the kinetics of cylinders to spheres transition in a block copolymer in a selective solvent using Brownian dynamics.

In Brownian dynamics, the effect of solvent on the polymer's motion is represented by a dissipative term and a random noise term instead of including the detailed motion of solvent molecules explicitly by solving the equations of motion of the solvent molecules.[28] The separation of time scales of polymer and solvent motion makes it possible to use a longer time step in the integration and significantly reduces computational time in simulating the polymer solution system. However, a limitation of the BD method used here is that it does not conserve momentum and thus the long-time behavior does not describe hydrodynamic behavior. Hydrodynamics have been included in simulations of block copolymers under shear (for example, Guo and Kremer[29] using MD with the momentum conserving DPD thermostat). Horsch *et al.*[22] compared BD with MD and DPD with momentum conserving thermostats to examine the issue of hydrodynamic interactions, and they show that the phases with greater than one-dimensional periodicity, such as hex cylinders, are formed in both cases. In view of this, we have adopted the simple BD approach in this paper to examine the mechanism of the transition from hex cylinders to spheres.

In the simulation, the system is coarse-grained such that the elemental unit is not a single molecule or even a single

[a)]This work is a part of Ph.D. dissertation of Minghai Li, Boston University, 2008.
[b)]Present address: Gustaf H. Carlson School of Chemistry and Biochemistry, Clark University, Worcester, Massachusetts 01610, USA.
[c)]Author to whom correspondence should be addressed. Electronic mail: rb@bu.edu.

 

monomer of the polymer, but rather a sphere representing the center of the mass of a cluster of many molecules. This sphere (denoted as monomer or bead in the later text) moves according to Newton's laws of motion.

Solvent selectivity further enriches the phase map and behavior of the block copolymers.[30,48] It is well known that in triblocks, it is possible to obtain either isolated or bridged micelles depending on whether the solvent prefers the outer A block or the inner B block.[31] It is also possible to produce inverted micelles with the majority component in the cores by using a solvent selective for the minority block.[32] We investigated the equilibrium phase diagram of ABA triblocks in both A and B selective solvents[33] and observed isolated as well as bridged micelles. In this paper, we report Brownian dynamics simulations to study the kinetics of the hex cylinders to fcc spheres transition in triblock copolymer solution systems by either instantaneously quenching the temperature, $T$, or changing the well-depth of Lennard-Jones (L-J) potential $\varepsilon$.

## II. SIMULATION MODEL

We simulated a symmetric triblock (ABA) copolymer in a selective solvent good for A block. The system consists of either 200 or 400 bead-spring chains in a cubic box. Each block of the copolymer chain has ten monomers of A or B, i.e., $A_{10}B_{10}A_{10}$, thus the total number of monomers in each triblock chain is 30 with a fraction of B monomers of 1/3. The A and B monomers are thermodynamically immiscible, thus the monomers of different types tend to separate from each other. A melt of such a triblock copolymer $A_{10}B_{10}A_{10}$ is similar in its behavior to the diblock $A_{10}B_5$ and thus expected to form the hex cylinders structure, with the minority B monomers forming the cylindrical cores embedded in the matrix of the majority A monomers.[34]

The potential energy associated with the interaction between nonbonded monomers is given by either the standard L-J 6–12 potential or the modified version, the Weeks–Chandler–Andersen (WCA) potential, depending on the types of interacting monomers. L-J potential is used for the interaction between B-B monomers, which includes the attractive term and repulsive term[35]

$$U_{\mathrm{L\text{-}J}} = 4\varepsilon\left[\left(\frac{\sigma}{r}\right)^{12} - \left(\frac{\sigma}{r}\right)^{6}\right] - 4\varepsilon\left[\left(\frac{\sigma}{r_c}\right)^{12} - \left(\frac{\sigma}{r_c}\right)^{6}\right],$$

$$r \le r_c = 2.5\sigma, \tag{1}$$

$$U_{\mathrm{L\text{-}J}} = 0, \quad r > r_c,$$

where $\sigma$ is the diameter of a bead (set to 1 in simulation), $\varepsilon$ is the well-depth of L-J potential, and the cutoff radius $r_c=2.5\sigma$. The aggregation of type B monomers is driven by nonzero well-depth, $\varepsilon$.

To describe the immiscibility between type A and B monomers, for A-B interactions, we use the repulsive WCA potential[36]

$$U_{\mathrm{WCA}} = 4\varepsilon\left[\left(\frac{\sigma}{r}\right)^{12} - \left(\frac{\sigma}{r}\right)^{6}\right] + \varepsilon, \quad r \le r_c = 2^{1/6}\sigma,$$

$$U_{\mathrm{WCA}} = 0, \quad r > r_c, \tag{2}$$

where the cutoff radius $r_c=2^{1/6}\sigma$. Here, the original L-J potential is truncated at its minimum $r_c=2^{1/6}\sigma$ and shifted up to 0, so that it is always positive and purely repulsive. The solvent interaction is treated implicitly. If the solvent is good to type A monomers, the WCA potential, instead of L-J potential, is used as type A-A interactions. The degree of immiscibility between A and B monomers and the quality of solvent selectivity is determined by the parameter $\varepsilon/k_BT$, where $T$ is temperature and $k_B$ is the Boltzmann constant.

The interaction between two neighboring bonded beads on a polymer chain is modeled by a finitely extensible nonlinear elastic (FENE) potential[19]

$$U_{\mathrm{FENE}} = -15\varepsilon\left(\frac{R_0}{\sigma}\right)^2 \ln\left[1 - \left(\frac{r}{R_0}\right)^2\right], \quad r < R_0 = 1.5\sigma,$$

$$U_{\mathrm{FENE}} = \infty, \quad r \ge R_0, \tag{3}$$

where $R_0$ is maximum allowable separation between two neighboring beads on the same chains. The FENE potential together with L-J or WCA potential yields a minimum potential at the separation $0.97\sigma$ for the two neighboring bonded beads on a polymer chain.

In the BD simulation, each bead is subjected to conservative forces $F_i^C$, friction forces $F_i^F$, and random forces $F_i^R$. The governing equation of motion[35] is $m\ddot{r}_i = F_i^C + F_i^F + F_i^R$, where $m$ is the mass of bead. The friction force is $F_i^F = -\gamma v_i = -6\pi\sigma\eta v_i$, where $\gamma$ is friction coefficient, $\eta$ is solvent viscosity, and $v$ is velocity of the bead. The random force $F_i^R$ arises from the random bombardment of solvent molecules and the effect of the thermal heat bath on the individual bead. The random force and friction force acting as hot and cold sources, respectively, constitute a nonmomentum conserving thermostat and obey the fluctuation dissipation theorem[18]

$$\langle F_i^R(t) F_j^R(t') \rangle = 6k_BT\gamma\delta_{ij}\delta(t - t'). \tag{4}$$

We applied periodic boundary conditions in all the simulations. The polymer volume fraction $\phi = NV_0/V$ was fixed during the simulation, where $N$ is total number of beads, $V_0 = \pi\sigma^3/6$ is the volume of an individual bead, and $V$ is the total system volume. The system size was chosen to be big enough to avoid finite size effects, yet not too large so as to obtain the equilibrium structure in a reasonable amount of computational time. The Verlet velocity method was applied and the time step $\Delta t = 0.01$ with the time unit $\sigma\sqrt{m/\varepsilon}$ was used to integrate the discretized equations of motion. A random configuration without any prior knowledge generated at high temperature was used as the initial configuration. Typically, the equilibrium configurations were obtained after running for $10^6$–$10^7$ time steps at the desired temperatures. The BD code used in this work is based on the code used in Professor Sharon Glotzer's group. Several simulations with different initial configurations were performed to avoid being

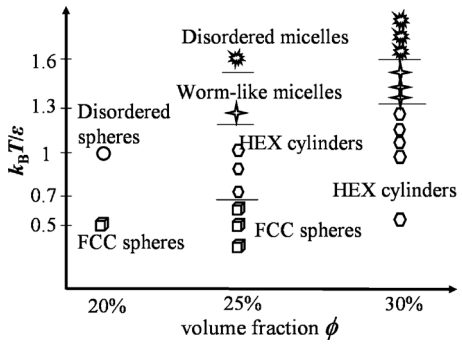


FIG. 1. The phase map showing structures observed in the simulation for $A_{10}B_{10}A_{10}$ in an A-selective solvent at different volume fractions and temperatures.

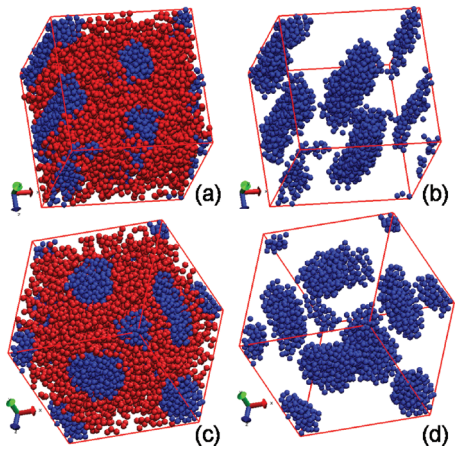


FIG. 2. Snapshots of various ordered structures of $A_{10}B_{10}A_{10}$ in the solvent poor to B in a cubic box ($23.25\sigma \times 23.25\sigma \times 23.25\sigma$) at volume fraction $\phi=25\%$. The monomer A is shown in red and B in blue. (a) hex cylinders formed by B monomers embedded in a matrix of A monomers at $T=0.8$ ($\varepsilon/k_B$). (b) For clarity, the same snapshot as (a) is shown with only B monomers displayed. (c) fcc spheres formed by B monomers embedded in A matrix at $T=0.5$ ($\varepsilon/k_B$). (d) The same snapshot as (c) is shown with only B monomers displayed for clarity.

trapped in a local energy minimum state. VISUAL MOLECULAR DYNAMICS[37] software was used for visualization of the morphology.

## III. RESULTS AND DISCUSSION

### A. Ordered structures and phase map in solvent selective for the outer block

We simulated the $A_{10}B_{10}A_{10}$ system at different temperatures for three different volume fractions $\phi=20\%$, 25%, and 30% in cubic boxes. Because BD is a very time consuming technique, it is not suitable to simulate the entire phase diagram with this technique. However, since the main goal of this paper is to study the kinetics, we only simulate the system at a few concentrations to identity the phase map. At each concentration, we simulated only one fixed box size. Because of this limitation, it is important to note that the structure may not represent the thermodynamic limit and lattice constants that we obtain may be dictated by finite size effects.

The phase map of observed morphologies for the three concentrations simulated in this work is shown in Fig. 1. All temperatures are given in units of $\varepsilon/k_B$. At $\phi=20\%$, we only observed fcc spheres at lower temperature $T=0.5$ and disordered spheres at higher $T=1$. At $\phi=25\%$, we observed fcc spheres at $T=0.6$ and below, and hex cylinders at $T=0.7$ and above. The phase boundary of hex and fcc is estimated as $T\sim 0.65$. At elevated temperatures, the cylinders bend and form wormlike micelles. At still higher temperatures, disordered micelles with ill-defined profiles are observed. At $\phi=30\%$, we observed hex cylinders for $T<1.3$, wormlike micelles at higher temperatures ($T=1.3$), and disordered ill-defined micelles at still higher temperatures ($T=1.6$). The snapshots of the hex cylinders and fcc spheres at $\phi=25\%$ at $T=0.8$ and 0.5, respectively, are shown in Fig. 2. The A monomer is shown in red and B monomers in blue in all the snapshots displayed in this text.

As mentioned earlier, the melt of $A_{10}B_{10}A_{10}$ forms cylinders with B in the cores, which would transform to bcc spheres at high temperatures. For $A_{10}B_{10}A_{10}$ in solvent selective to outer A-block system, because solvent is poor to the minority B block, the selectivity of the solvent further enhances the microphase separation tendency due to the incompatibility of A and B blocks. Thus we expect to obtain cylindrical or spherical micelles with the inner B blocks in the cores and the outer A blocks, forming the solvated corona under certain concentrations and temperatures.

We also studied the triblock copolymers $A_5B_{20}A_5$ and $A_{10}B_{10}A_{10}$ in a solvent selective to the inner B block. For the $A_5B_{20}A_5$ system at $\phi=35\%$, hex cylinders and fcc spheres which are linked by the B chains are observed at $T=0.7$ and 0.5, respectively. For the $A_{10}B_{10}A_{10}$ system at $\phi=30\%$, LAM and hexagonally perforated lamellar ordered structures are obtained at $T=1$ and 0.5, respectively.

The existence of fcc lattice of spherical micelles in block copolymer melt has been predicted theoretically.[38,39] For example, using the self-consistent field theory, Matsen and Bates[40] predicted a close-packed spheres (CPS) packed into fcc or hexagonal close-packed (hcp) lattice to exist in a narrow region between bcc spheres and disordered phase in the phase diagram. However, such CPS morphology has not been identified experimentally in block copolymer melt so far. This may be due to the fact that the thermal fluctuations destabilize the long-range order of CPS and give rise to the disordered micelles.[41–43] The addition of selective low molecular weight solvent or homopolymer to the block copolymer gives rise to additional phase behaviors on the system. Recently, Anderson *et al.*[20] used MD simulation to study the micellar crystals of triblock copolymer solution $A_nB_mA_n$ (A is hydrophilic and B is hydrophobic), and found both bcc and fcc structures depending on the box size and the composition of the triblock. Their studies of the system of $A_6B_7A_6$, which is close to our system, also showed that the hex cylindrical micelles are formed in the higher volume fraction and fcc spherical micelles are formed at lower volume fraction and lower kinetic temperatures for triblocks with short hydrophilic blocks. The results agree with our simulations shown in Fig. 1, although slightly different forms of the hydrophilic interactions and bonded interactions were used. Experimentally, a stable fcc phase of spherical micelles has been reported in block copolymer solution systems,[44–51] as well as

in block copolymer/homopolymer blends.[50] McConnell *et al.*[44] studied poly(styrene-*b*-isoprene) (SI) in decane, a selective solvent to polyisoprene (PI), and observed the fcc and bcc spheres phase. They found that the formation of fcc or bcc phase depends on the length of coronal layer thickness relative to the core radius, i.e., spherical micelles with thinner corona layer favors fcc phase due to the short-range intermicellar repulsions, whereas for "soft spheres" with thicker coronal layer, bcc phase is favored. Hanley *et al.*[48] investigated the SI 20% in diethyl phthalate (DEP), a selective solvent to polystyrene but poor for PI, and identified the fcc spheres phase at low temperature which transforms into hex cylinders phase upon heating with the transition temperature of ~100 °C. Recently, Park *et al.*[49] studied the SI in DEP solution system with different concentration and molecular weight and found the coexistence of fcc and hcp of spheres at low temperature. On increasing temperature, the system transforms from fcc/hcp spheres → bcc/hcp spheres → hex cylinders.

McConnell *et al.*[44] found that the formation of lattice structure of spherical micelles depends on $\xi=\langle L\rangle_h/R_c$, the ratio of the coronal layer thickness ($\langle L\rangle_h$) to the radius of the core ($R_c$). According to the phase diagram presented in Ref. 44, for $\xi<1.5$, the system favors the formation of fcc lattice, whereas for the $\xi>1.5$, the formation of bcc lattice is favored. In our simulation at $\phi=25\%$ and $T=0.5$, the radius of the sphere is estimated as $R_c/\sigma=5.6\pm0.5$ by directly measuring the diameters of the cores from the simulations by using the software ATOMEYE[52] to visualize the domains and rotating them. Since the domains are not perfect spheres, but ellipsoidal, the average of the major and minor radius was used to determine an effective radius. The thickness of the coronal layer is estimated by subtracting the core radius from half of the nearest-neighbor distance $d=16.5\sigma\pm1.0\sigma$, i.e., $\langle L\rangle_h/\sigma=d/2-R_c\approx2.6$. Thus $\xi=\langle L\rangle_h/R_c\approx0.5$.[53] Since the ratio $\xi\approx0.5$ lies in the region of fcc in the phase diagram, the observation of fcc lattice in our simulation is exactly as predicted.[44]

### B. Kinetics of hex to fcc transition

#### 1. Time evolution of structure following temperature quench

To investigate the kinetics of the transition from hex cylinders to fcc spheres for the system of $A_{10}B_{10}A_{10}$ in the A-selective solvent, simulations with longer cylinders were carried out with initial configuration generated by repeating the box of Fig. 2(a) twice along the cylinder axis dimension (y axis), thereby doubling the length of the cylinders. The kinetics was simulated in a rectangular box of $23.25\sigma\times46.5\sigma\times23.25\sigma$ at the volume fraction 25% by instantaneously quenching the temperature from 0.8 to 0.5, with a fixed well-depth of L-J $\varepsilon=1$.

At $T=0.8$, the system is in the hex cylinder ordered structure [Fig. 2(a)]. Following the quench, we run the simulation at low $T=0.5$ until the fcc structure is obtained. The time evolution of the developing morphology for hex cylinders to fcc spheres transition is shown in Fig. 3. Each cylinder of the initial configuration is indexed with a number as shown in the inset of Fig. 3.

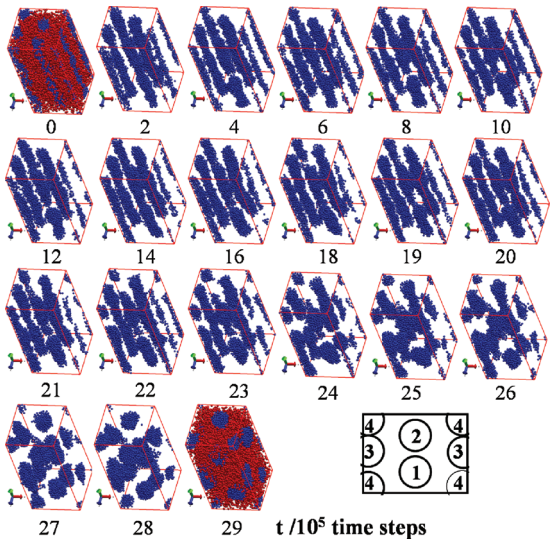


FIG. 3. Time sequence of morphology evolution of $A_{10}B_{10}A_{10}$ for hex cylinders to fcc transition following a temperature jump from 0.8 to 0.5 (with $\varepsilon=1$) in a rectangular box with the size of $23.25\sigma\times46.5\sigma\times23.25\sigma$ at volume fraction $\phi=25\%$. Time is indicated in the scale of $10^5$ time steps. The right bottom inset shows the index numbers of all four cylinders of the initial configuration from the top view. A is removed for clarity for some of the snapshots.

At time $t=0$, corresponding to the instantaneous quench moment, the system was in the hex cylinder phase. At $t=2\times10^5$ time step, one cylinder showed a ripple, indicating the beginning of the breakup into spheres. At $t=3\times10^5$ time step, the cylinder indexed 1 broke and induced the neighboring cylinders to ripple. The neighboring cylinder 4 broke at $22\times10^5$ time step and all the rest of cylinders broke at $24\times10^5$ time step at different positions along the cylinder axis. At $t=29\times10^5$ time step, the broken domains became spherical and lay on a fcc lattice. It appears that after the cylinders broke up, the spheres rearranged slightly to the fcc lattice.

The results shown in Fig. 3 are consistent with nucleation and growth mechanism of the transition from cylinders to spheres. In the nucleation and growth scenario, the cylinders are metastable with respect to the modulation; thus, some parts of the cylinders would develop ripples while others would remain intact, and the front of the modulation would advance with time along the cylinder axis, as described by Matsen.[13] The ripples would induce rippling in the neighboring cylinders. In contrast, in the spinodal decomposition scenario, the cylinders are unstable with respect to the modulation, hence ripples form over the entire length of the cylinders. Additionally, if the modulations are correlated with neighboring cylinders, the epitaxial transition is possible.

To see more clearly how one cylinder transforms to spheres, cylinder 1 is extracted and the time sequence of the snapshots of its profile is shown in Fig. 4. At $t=2\times10^5$ time step the cylinder began to pinch at its middle and at $3\times10^5$ time step, it broke. Small fluctuations of the rest of

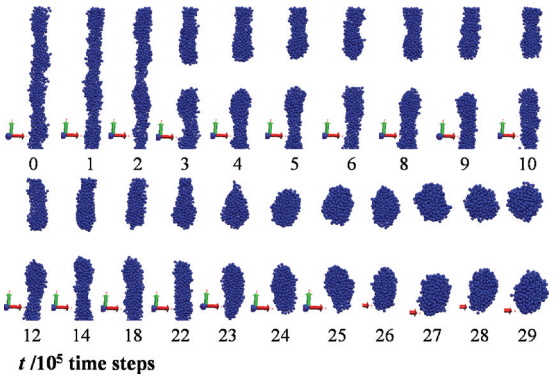


FIG. 4. Time sequence of snapshots for the profile of the cylinder 1 extracted from Fig. 3. Time is indicated in the scale of $10^5$ time steps.

the cylinder were present until $t=22\times10^5$ time step, when the ripples on the rest of the cylinder began to grow. The cylinder eventually broke up into two ellipsoidal clusters at $t=23\times10^5$ time step. The two clusters became spherical at $t=29\times10^5$ time step.

The simulation results described above are qualitatively in agreement with our previous paper[8] supporting the ripple mechanism for the hex cylinders to bcc spheres phase transition in poly(styrene-*b*-ethylene-*co*-butylene-*b*-styrene) in mineral oil, a selective solvent for the middle block, using time-resolved small angle x-ray scattering following various temperature jumps. At a concentration of 45%, this system exhibits a hex cylinder phase at lower temperature and undergoes an OOT from hex cylinders to bcc spheres upon heating. We observed that the transition occurred via a nucleation and growth mechanism for a shallow temperature jump and a spinodal decomposition mechanism with continuous ordering for a deep temperature jump. The scattering data were found to be in good agreement with scattering profiles calculated using a model rippled cylinder form factor and the phases between adjacent cylinders chosen to satisfy the epitaxial relationship.[8]

### C. Density profiles

To quantitatively study the structural development during the transformation process, we calculate the density profile of each cylinder in the following way: all the A monomers that are good to solvent in a given cylinder are extracted out; then the remaining B monomers are binned into different sections according to the position of center of each monomer along the cylinder axis (y axis in this case), and the number of B monomers falling into each section is taken as the density profile for that section number. This density profile is plotted in Fig. 5. One can see from Fig. 5(a) that cylinder 1 breaks up at y $\sim25\sigma$ at $t=3\times10^5$ time step; at the same time two peaks appear in the density profile at y $\sim17\sigma$ and $37\sigma$, respectively. The peaks grow becoming better defined as time increases and their positions shift toward the two ends of the cylinder. At around $t=22-23\times10^5$ time step, a region of depleted density appears and begins to grow. This observation is consistent with the snapshots displayed in the Fig. 4. From the density profile of the adjacent cylinder 2, shown in Fig. 5(b), we see that

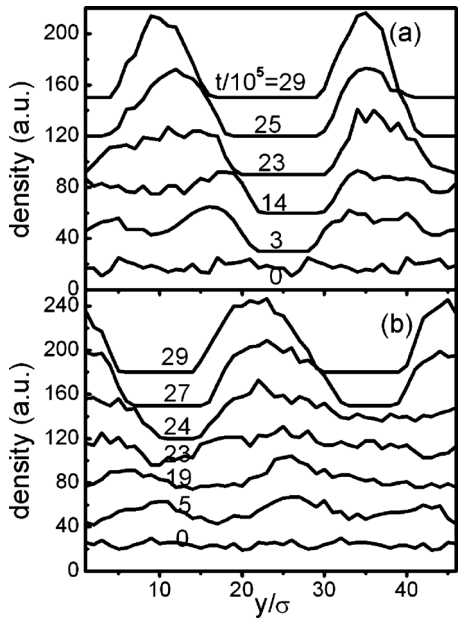


FIG. 5. Time evolution of density profiles of two cylinders, following a temperature quench from 0.8 to 0.5: (a) for cylinder 1 and (b) for cylinder 2. The data are shifted vertically for clarity. Time is indicated in the scale of $10^5$ time steps.

the fluctuations in the density profile appear at later time as compared to cylinder 1, and the positions of the peaks lie in the depletion regions of cylinder 1, implying that the spherical domains in cylinder 2 develop in the regions where cylinder 1 is pinching off, consistent with the epitaxial nature of the transformation.

The density profiles of cylinders 3 and 4, which are not shown here, have the similar time evolution behaviors to cylinder 2. It also can be seen from the density profiles that the four cylinders ripple and break up in a cooperative way at the different positions along the cylinder axis. All observations are in good agreement with scenario depicted in the nucleation and growth mechanism.

### D. Fourier transform of pair density distribution

The Fourier transform of the pair density distribution, i.e., the scattering intensities of configurations, is calculated in two steps. First, the structure factor is given by $S(\vec{q})=|\Sigma_{j\in B}(-i\vec{q}\cdot\vec{r}_j)|^2$, where $\vec{q}$ is scattering vector and $\vec{r}_j$ is position vector of B-type monomer. The sum is made only over all B-type monomers and the scattering contributed from A-type monomers is regarded as the background. Second, the azimuthally average scattering intensity $I(q)$ is calculated by numerical integration of $S(\vec{q})$ over the angular space as $I(q)=\int S(\vec{q})\cdot d\Omega/4\pi$, where $d\Omega$ is the element of solid angle. The results are shown in Fig. 6. The first three peaks at $t=0$ are in good agreement with hex predictions (with relative peak positions $1:\sqrt{3}:\sqrt{4}$) and the first four peaks at $t=29\times10^5$ time step are also in good agreement with fcc predictions (with relative peak positions $1:\sqrt{4/3}:\sqrt{8/3}:\sqrt{11/3}$). From Fig. 6, one can see that as time increases, small changes in scattering intensity are present until $t=24\times10^5$ time step, when a new peak emerges and grows in the primary peak region, indicating a dramatic

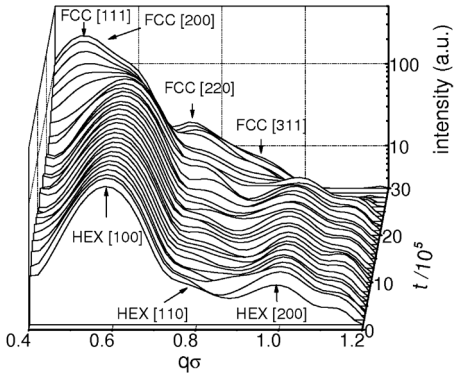


FIG. 6. Time evolution of Fourier transform of the pair density distribution following a temperature quench from 0.8 to 0.5. Time is indicated in the scale of $10^5$ time steps. The first few relative peak positions for hex and fcc are marked.

change in the transition process. This is consistent with the observation from the snapshot shown in Fig. 3, where at $t=24\times10^5$ time step, all four cylinders break and some spheres are about to appear on a fcc lattice.

The Fourier transform shows two distinct primary peaks coexisting: $I_{[100],\mathrm{hex}}$, i.e., hex [100] Bragg peak and $I_{[111],\mathrm{fcc}}$ for fcc [111] Bragg peak. The time evolutions of the peaks intensities, $I_{[100],\mathrm{hex}}$ and $I_{[111],\mathrm{fcc}}$ are plotted in Fig. 7. As expected, $I_{[100],\mathrm{hex}}$ decreases and $I_{[111],\mathrm{fcc}}$ increases in a stretched exponential way, both of which can be well fitted by the Avrami equation, which is often used to describe the nucleation and growth process

$$I(t)-I(t_0)=(I(t_\infty)-I(t_0))(1-e^{-((t-t_0)/\tau)^n}). \quad (5)$$

The fitting results are also shown in Fig. 7. The exponent $n$ of the Avrami equation equals 2.5 for hex and 3.2 for fcc.

Although there is no study of the hex to fcc kinetics in the literature, Nie[54] measured the reverse transition from fcc spheres to hex cylinders in SI 40% w/v in dimethyl phthalate, a selective solvent to polystyrene. This diblock solution system exhibits an OOT from fcc spheres to hex cylinders upon heating with transition temperature of 110 °C. Two stages were observed in the experimental study. The early stage was described well by an Avrami equation,[55] i.e., a stretched exponential growth which could be fit with an exponent $n=3$ or 4, indicating that the growth of hex from fcc involves a two-dimensional or three-dimensional

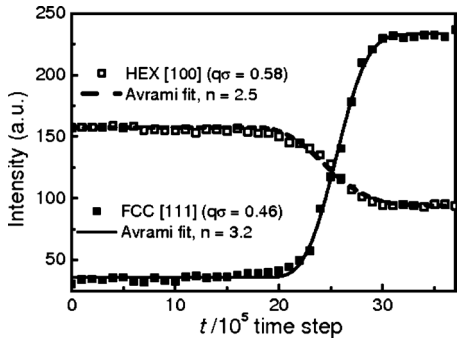


FIG. 7. Time evolution of the intensities of primary peaks for hex and fcc, following a temperature quench from 0.8 to 0.5. The results of Avrami fitting are shown with lines.

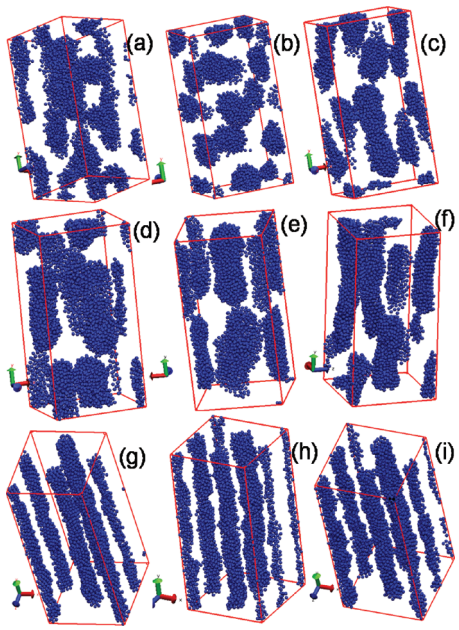


FIG. 8. The snapshots of various $\varepsilon$ jumps for $A_{10}B_{10}A_{10}$ at fixed $T=0.8$, $\phi=25\%$. All initial $\varepsilon=1$. (a) $\varepsilon$ jump to $\varepsilon_f=1.25$, at $t=10^7$ time step; (b) for $\varepsilon_f=1.5$, at $t=3\times10^6$ time step; (c) for $\varepsilon_f=1.75$, at $t=10^7$ time step; (d) for $\varepsilon_f=2$, at $t=10^7$ time step; (e) for $\varepsilon_f=2.5$, at $t=10^7$ time step; (f) for $\varepsilon_f=3$, at $t=10^7$ time step; (g) for $\varepsilon_f=4$, at $t=10^7$ time step; (h) for $\varepsilon_f=8$, at $t=10^7$ time step; and (i) for $\varepsilon_f=10$, at $t=10^7$ time step.

mechanism.[56] However, the exponents for the reverse transition need not be the same as those reported for the fcc to hex transition. The overall behavior of the primary peaks agrees well with the first stage reported by Nie[54] but no second stage is observed in the simulations because the system simulated here is too small to observe the growth and coarsening of fcc microdomains observed in the experiments.

### E. Simulations following jumps of well-depth of L-J potential

An alternative approach to investigate the kinetics of hex cylinders to fcc transition is to instantaneously jump the well-depth of L-J potential $\varepsilon$. During the simulation, the value of $T$ is fixed so that the jump does not change the average speed of monomers, thus it saves computation time. Indeed, the effect on thermodynamic behavior of increasing the value of $\varepsilon$ is equivalent to decreasing the value of $T$ because the temperature is measured in the scale of $\varepsilon/k_B$.

We started from the initial configuration of hex cylinders for $A_{10}B_{10}A_{10}$ at $T=0.8$, $\phi=25\%$, $\varepsilon=1$, as in the temperature jump study. We run the simulation following an instantaneous jump of $\varepsilon$ from 1 to various higher values $\varepsilon_f=1.25-10$, while fixing value of $T=0.8$. The snapshots of the configurations for all $\varepsilon$-jumps after running for certain time steps are shown in Fig. 8.

For $\varepsilon$-jump to $\varepsilon_f=1.25$, as shown in Fig. 8(a), one cylinder broke up and formed spheres and the other formed ripples at $t=10^7$ time step. Thus, it was still in the intermediate stage at this time and undergoing further transition.

For $\varepsilon$-jump to $\varepsilon_f=1.5$, as shown in Fig. 8(b), the system formed the fcc earlier than $3\times10^6$ time steps. For $\varepsilon$-jump to $\varepsilon_f=1.75$, at $t=10^7$ time step, as shown in Fig. 8(c), the cyl-

inders are broken. Some of these broken cylinders formed spheres and others formed the short cylinders which may change into spheres at a longer time. In contrast to these cases, for $\varepsilon$-jump to $\varepsilon_f=2$, at $t=10^7$ time step, as shown in Fig. 8(d), the cylinders broke up and formed short cylinders which persisted for a longer time. For $\varepsilon$-jump to $\varepsilon_f=2.5$ and 3, as shown in Figs. 8(e) and 8(f), the behaviors are similar to that of the $\varepsilon$-jump to 2. In these cases, however, the resulting cylinders are a little longer. For $\varepsilon$-jump to $\varepsilon_f=4$, as shown in Fig. 8(g), the cylinders are still all intact even at $t=10^7$ time step and remain intact for longer time. For jump to higher $\varepsilon$ such as $\varepsilon_f=8$ and 10, as shown in Figs. 8(h) and 8(i), the behavior is similar to the jump of $\varepsilon$ to 4. The simulation time step is chosen to be 0.005 for the latter two systems.

From the snapshots for the various $\varepsilon$-jumps simulated in this work shown in Fig. 8, one can see the existence of an optimum jump to $\varepsilon_f \approx 1.5$, where the transition of hex cylinders to fcc spheres occurs quickly via the nucleation and growth mechanism. For $\varepsilon$-jump to a value below this optimum, such as $\varepsilon_f=1.25$, the transition occurs slowly because the corresponding temperature $k_BT/\varepsilon_f=0.64$ is close to the phase boundary, which slows down the kinetics. The phase boundary of hex and bcc is estimated as ~0.65 (see Fig. 1). For $\varepsilon$-jump to a value above 1.5 but less than 2, such as $\varepsilon_f=1.75$, the transition occurs slower than $\varepsilon_f \approx 1.5$ and it takes a longer time to complete the transition. For $2 \leq \varepsilon_f \leq 3$, the cylinders break up but form short cylinders instead of spheres, and the transition is not completed within our computational time limit. For large $\varepsilon_f \geq 4$, the cylinders do not break up within our computational time limit and the structure is kinetically trapped. Therefore, the rate of the transformation has an optimal value for $\varepsilon_f$ which is neither close to the phase boundary, nor involved with deep trapping basins. Experimentally, the phase separation is also faster in the vicinity of the cloud point as compared to the vicinity of the coexistence curve.

## IV. CONCLUSION

In this paper, we report Brownian dynamics simulation to study the kinetics of hex cylinders to fcc spheres transition in triblock copolymer $A_{10}B_{10}A_{10}$ in an A-selective solvent, following an instantaneous temperature quench or jumps of well-depth of L-J potential. We determined the equilibrium phases of hex cylinders and fcc spheres at temperature $T=0.8$ and 0.5 ($\varepsilon/k_B$), respectively, at the volume fraction $\phi=25\%$. We then use the hex cylinders as initial configuration and quench the temperature from 0.8 to 0.5 while fixing $\varepsilon$ to study the kinetics of the transition from hex cylinders to fcc spheres. The snapshots and density profiles evaluated during the hex to fcc transition show that initially, one cylinder breaks at its middle part and the front of the ripple begins to advance to the rest of the cylinder. The initial ripple induces the formation and development of ripples of the neighboring cylinders. The Fourier transform of pair density distribution indicates a dramatic change at $t=24\times10^5$ time step, which is consistent with the observation from the snapshots that at this moment all the cylinders break up and the spheres are about to appear on the fcc lattice. These observations agree well with the nucleation and growth mechanism.

The kinetics of this transition was also investigated by suddenly changing the well-depth of L-J potential $\varepsilon$ from 1 to various higher values while fixing the value of $T=0.8$. We found the rate of the transformation has an optimum for $\varepsilon$-jump to $\varepsilon_f \approx 1.5$ which is neither close to the phase boundary, nor involved with deep trapping basins. At lower $\varepsilon_f$ ($<1.5$), the quench is close to the phase boundary, which slows down the kinetics; at very higher $\varepsilon_f$ ($\geq 4$), the structure is kinetically trapped.

## ACKNOWLEDGMENTS

This research was supported by the National Science Foundation, Division of Materials Research (Grant No. NSF-DMR 0804784). We acknowledge the support of Boston University's Scientific Computation and Visualization group, also supported by NSF for computational resources. We thank Professor Sharon Glotzer for providing us the original code which was modified for this study. We also thank Professor Bill Klein, Professor Chi Wu, Dr. Zhenli Zhang, Dr. Zhenhua Wu, Dr. Rachele Dominguez, and Dr. Kipton Barros for helpful discussions.

[1] I. W. Hamley, *The Physics of Block Copolymers* (Oxford University Press, New York, 1998).
[2] N. Hadjichristidis and S. Pispas, *Block Copolymers: Synthetic Strategies, Physical Properties, and Applications* (Wiley, New York, 2002).
[3] F. S. Bates and G. H. Fredrickson, Annu. Rev. Phys. Chem. **41**, 525 (1990).
[4] Y. Liu, M. Li, R. Bansil, and M. Steinhart, Macromolecules **40**, 9482 (2007).
[5] S. Sakurai, H. Kawada, T. Hashimoto, and L. J. Fetters, Macromolecules **26**, 5796 (1993).
[6] K. Kimishima, T. Koga, and T. Hashimoto, Macromolecules **33**, 968 (2000).
[7] J. K. Kim, H. H. Lee, M. Ree, K. B. Lee, and Y. Park, Macromol. Chem. Phys. **199**, 641 (1998).
[8] M. Li, Y. Liu, H. Nie, R. Bansil, and M. Steinhart, Macromolecules **40**, 9491 (2007).
[9] X. Y. Cheng, L. Lin, E. Weinan, P. W. Zhang, and A. C. Shi, Phys. Rev. Lett. **104**, 148301 (2010).
[10] M. Laradji, A. C. Shi, J. Noolandi, and R. C. Desai, Macromolecules **30**, 3242 (1997); M. Laradji, A. C. Shi, R. C. Desai, and J. Noolandi, Phys. Rev. Lett. **78**, 2577 (1997).
[11] A. Ranjan, J. Qin, and D. C. Morse, Macromolecules **41**, 942 (2008).
[12] A. C. Shi, J. Phys.: Condens. Matter **11**, 10183 (1999).
[13] M. W. Matsen, J. Chem. Phys. **114**, 8165 (2001).
[14] M. Nonomura and T. Ohta, Physica A **304**, 77 (2002).
[15] S. Qi and Z. G. Wang, Phys. Rev. Lett. **76**, 1679 (1996); Phys. Rev. E **55**, 1682 (1997).
[16] A. M. Mayes and M. Olvera de la Cruz, J. Chem. Phys. **95**, 4670 (1991).
[17] M. Murat, G. S. Grest, and K. Kremer, Macromolecules **32**, 595 (1999).
[18] G. S. Grest, M.-D. Lacasse, K. Kremer, and A. M. Gupta, J. Chem. Phys. **105**, 10583 (1996).
[19] G. S. Grest and K. Kremer, Phys. Rev. A **33**, 3628 (1986); J. W. Rudisill and P. T. Cummings, Rheol. Acta **30**, 33 (1991).
[20] J. A. Anderson, C. D. Lorenz, and A. Travesset, J. Chem. Phys. **128**, 184906 (2008).
[21] A. J. Schultz, C. K. Hall, and J. Genzer, J. Chem. Phys. **117**, 10329 (2002).
[22] M. A. Horsch, Z. Zhang, C. R. Lacovella, and S. C. Glotzer, J. Chem. Phys. **121**, 11455 (2004).
[23] U. S. Agarwal, R. Bhargava, and R. A. Mashelkar, J. Chem. Phys. **108**, 1610 (1998).
[24] G. Besold, O. Hassager, and O. G. Mouritsen, Comput. Phys. Commun. **121–122**, 542 (1999).
[25] A. Hoffmann, J. U. Sommer, and A. Blumen, J. Chem. Phys. **106**, 6709

(1997); **107**, 7559 (1997).
[26] R. G. Larson, Macromolecules **27**, 4198 (1994); J. Chem. Phys. **96**, 7904 (1992).
[27] R. D. Groot and T. J. Madden, J. Chem. Phys. **108**, 8713 (1998).
[28] S. C. Glotzer and W. Paul, Annu. Rev. Mater. Res. **32**, 401 (2002).
[29] H. Guo and K. Kremer, J. Chem. Phys. **119**, 9308 (2003); H. Guo, *ibid.* **124**, 054902 (2006); H. Guo and K. Kremer, *ibid.* **127**, 054902 (2007).
[30] T. P. Lodge, B. Pudil, and K. J. Hanley, Macromolecules **35**, 4707 (2002).
[31] N. P. Balsara, M. Tirrell, and T. P. Lodge, Macromolecules **24**, 1975 (1991).
[32] Q. Zhang, O. K. C. Tsui, B. Du, F. Zhang, T. Tang, and T. He, Macromolecules **33**, 9561 (2000).
[33] M. Li, Ph.D. dissertation, Boston University, 2008.
[34] M. W. Matsen and R. B. Thompson, J. Chem. Phys. **111**, 7139 (1999).
[35] M. P. Allen and D. J. Tildesley, *Computer Simulation of Liquids* (Clarendon, Oxford, 1987).
[36] J. D. Weeks, D. Chandler, and H. C. Andersen, J. Chem. Phys. **54**, 5237 (1971).
[37] See http://www.ks.uiuc.edu/Reseach/vmd/ for VMD.
[38] M. W. Matsen and F. S. Bates, Macromolecules **29**, 1091 (1996).
[39] A. N. Semenov, Macromolecules **22**, 2849 (1989).
[40] M. W. Matsen and F. S. Bates, J. Polym. Sci., Part B: Polym. Phys. **35**, 945 (1997); M. W. Matsen and M. Schick, Phys. Rev. Lett. **72**, 2660 (1994).
[41] A. Brazovskii, Sov. Phys. JETP **41**, 85 (1975).
[42] G. H. Fredrickson and E. Helfand, J. Chem. Phys. **87**, 697 (1987).
[43] E. E. Dormidontova and T. P. Lodge, Macromolecules **34**, 9143 (2001).
[44] G. A. McConnell, A. P. Gast, J. S. Huang, and S. D. Smith, Phys. Rev. Lett. **71**, 2102 (1993); G. A. McConnell and A. P. Gast, Phys. Rev. E **54**, 5447 (1996).
[45] J. F. Berret, F. Molino, G. Porte, O. Diat, and P. J. Lindner, J. Phys.: Condens. Matter **8**, 9513 (1996).
[46] O. Diat, G. Porte, and J. F. Berret, Phys. Rev. B **54**, 14869 (1996).
[47] J. A. Pople, I. W. Hamley, J. P. A. Fairclough, A. J. Ryan, B. U. Komanschek, A. J. Gleeson, G.-E. Yu, and C. Booth, Macromolecules **30**, 5721 (1997).
[48] K. J. Hanley, T. P. Lodge, and C.-I. Huang, Macromolecules **33**, 5918 (2000).
[49] M. J. Park, J. Bang, T. Harada, K. Char, and T. P. Lodge, Macromolecules **37**, 9064 (2004).
[50] Y. Y. Huang, H. L. Chen, and T. Hashimoto, Macromolecules **36**, 764 (2003).
[51] P. Sakya, J. M. Seddon, R. H. Templer, R. J. Mirkin, and G. J. T. Tiddy, Langmuir **13**, 3706 (1997).
[52] J. Li, Modell. Simul. Mater. Sci. Eng. **11**, 173 (2003).
[53] The ratio $\xi$ is estimated by another approach using the volume of the spheres to calculate the effective radius of the cores. The core radius $R_c = \sqrt[3]{N/f} \cdot r_0$, where $N=400-600$ beads in a sphere, $f$ is the maximum packing fraction equals 0.74 (for fcc or hcp packing), and $r_0=\sigma/2$ is the radius of bead. This gives $R_c/\sigma=4.4\pm0.3$, which is underestimated and smaller than the direct measurement because the beads inside the spheres are not close-packed. The coronal layer thickness can also be estimated by the end-to-end distance of the outer block assuming they are self-avoiding walk chains, i.e., $\langle L\rangle_h=10^{0.6}\sigma\approx4\sigma$. Thus, $\xi=\langle L\rangle_h/R_c\approx0.9$. Although this value is an overestimate, it is less than 1.5, which favors the formation of fcc structure.
[54] H. Nie, Ph.D. dissertation, Boston University, 2005, p. 125.
[55] M. Avrami, J. Chem. Phys. **7**, 1103 (1939); M. J. Avrami, *ibid.* **8**, 212 (1940); M. Avrami, *ibid.* **9**, 177 (1941).
[56] J. M. Schultz, *Polymer Crystallization* (Oxford University Press, New York, 2001), p. 179.